Partially coherent quasi-Airy beams with controllable acceleration

Zihao Pang, Xiaoyan Zhou, Zhenglin Liu, and Daomu Zhao [*]

Zhejiang Province Key Laboratory of Quantum Technology and Device, Department of Physics, Zhejiang University, Hangzhou 310027, China

Self-acceleration and nondiffraction can be considered as the new properties of partially coherent light beams nowadays, provided that the light source is properly chosen and modulated. Here, we introduce a class of partially coherent light beams the propagation trajectory of which performs a parabolic-type curve as the well-known Airy beams. Theoretically, they are originated from a well-designed cross-spectral density function in the spatial-frequency domain. Experimentally, they are produced by shining an amplitude-modulated Schell-model source on the phase mask which is the Fourier transform of predesigned Airy functions. It is shown that, for such beams, one can control their acceleration properties by adjusting the initial angle of the sidelobes. Moreover, when the source is under a nearly incoherent state, the oscillation of the sidelobes of the beams turns smooth and the intensity distribution concentrates on the mainlobe with the Airy tails. The experimental results are in agreement with the theoretical predictions. A trial solution for coherent-mode representation of such a beam is derived and our paper provides an alternative outlook for understanding of self-acceleration on partially coherent light beams.

I. INTRODUCTION

Lasers, as a vital light source in modern optics, possess the fundamental characteristic of high spatial coherence resulting from stable oscillation in the optical resonant cavity. As we know, such a high degree of spatial coherence can bring increasingly bright illumination and extremely directional emission. In some fields like optical imaging, however, a high degree of spatial coherence may be considered as a drawback to an imaging system [1–3], due to the coherent artifacts (such as speckle) from the intense interference at the detector. Atop this background, the concept of partially coherent light sources [4] with low spatial coherence thus has been introduced by using the modulation of the degree of coherence (DOC) function. In late 1970s, it was found [5] that, for a partially coherent field, this kind of modulation in the near field enables the control of beam shaping in the far field. Subsequently, the beam shaping of partially coherent light beams has raised the attention of the optics community and experienced a rapid development over the years [6]. Provided that the DOC function of the source is properly designed, the intensity distribution of the light beam in the far field can acquire many intriguing physical phenomena, for example, the coherence vortex [7–12], optical coherence lattices [13,14], and even blueshift and redshift at the propagating spectra [15].

Since the realization of Airy beams with low spatial coherence [16–18], one is now able to sculpture a partially coherent light beam with the properties of self-acceleration and nondiffraction. It is important and inspiring for us to review the previous work. The earlier investigations suggest that there used to be three means of generating partially

coherent Airy beams: the cubic-phase modulation of a broadband light source in the spatial frequency domain [19], the ensemble average of Airy beams by propagating through random media [20], and the appropriate design of the DOC function for Airy beams in the spatial domain [21]. Such treatments, however, have been found to bring the sharply reduced acceleration range of the Airy beam under a nearly incoherent state. In recent years, partially coherent single [18] and multiple [22] Airy beams are realized by replacing Gaussian beams with monochromatic Gaussian Schell-model beams as light sources. These two versions, different from the earlier cases, have been proven to retain the identical accelerating property as their coherent counterparts.

On the other hand, for the case of fully coherent light fields, it has been found that some fascinating light beams can be derived by the specific design of the Airy function at the input of the optical system. For instance, circular Airy beams with an abruptly autofocusing feature are proposed by assembling the Airy function in the radial direction of cylindrical coordinates [23–25]; accelerating self-imaging along curved trajectories induced by Airy-Talbot effect can be engineered by a flexible superposition of Airy wave functions [26,27]. Here, we present, theoretically and experimentally, a kind of partially coherent light beam with controllable acceleration. They are generated by imposing the Schell-model correlation on the spectrum of quasi-Airy beams [28,29] in the spatial-frequency domain. In order to avoid confusion with the incoherent self-accelerating beams demonstrated in [18], we use the term "partially coherent quasi-Airy" (PCQA) beams for the proposed beams in this paper.

The organization of the paper is as follows. In Sec. II, we introduce the theoretical model; in Sec. III, we gain a deeper understanding of PCQA beams from the perspective of their coherent-mode representation; in Sec. IV, we perform the

*zhaodaomu@yahoo.com

experimental realization of the beams; in Sec. V, we conclude the paper.

II. THEORETICAL MODEL

In the section, we first build the radiation model of PCQA beams and study their propagation properties in free space. By mathematically constructing two one-dimensional Airy functions with arbitrary geometrical orientations in the spatial domain, fully coherent quasi-Airy (FCQA) beams at $z = 0$ are defined as [28,29]

$$
\phi_i(x, y) = \text{Ai}[\xi(x, y)]\text{Ai}[\eta(x, y)]
$$
$$
\times \exp\{(\alpha + i\beta)[\xi(x, y) + \eta(x, y)]\} \quad (1)
$$

with separately rotated dimensionless transverse coordinates:

$$
\xi(x, y) = \frac{x}{w_0}\cos\frac{\varphi}{2} + \frac{y}{w_0}\sin\frac{\varphi}{2},
$$
$$
\eta(x, y) = \frac{x}{w_0}\sin\frac{\varphi}{2} + \frac{y}{w_0}\cos\frac{\varphi}{2}, \quad (2)
$$

where $\text{Ai}(\cdot)$ is the Airy function [30]; $\varphi = \theta - \pi/2$ with $\pi/2$ being the factor that ensures the beams accelerate along the $+x$ and $+y$ directions; θ is regarded as the initial angle between the two lobes since it is reported that such an angle in FCQA beams occurs only at the initial plane ($z = 0$); w_0 is the transverse size; α is the decay parameter [16,17]; and β is known as the linear chirp coefficient controlling the incident angle of the beams [31,32].

Similar to the well-known Airy beams, the light beams described in Eq. (1) can also be achieved in experiment with the method of Fourier transform. Then, after omitting the higher-order terms and selecting $\beta = 0$ for simplicity, the Fourier spectrum $\widetilde{\phi}_s(k_x, k_y)$ of Eq. (1) is proportional to

$$
\widetilde{\phi}_s(k_x, k_y) \propto \exp\left[-\frac{\alpha}{2}[\xi^2(k_x, k_y) + \eta^2(k_x, k_y)]\right]
$$
$$
\times \exp\left[\frac{ic_0^3}{3}[\xi^3(k_x, k_y) + \eta^3(k_x, k_y)]\right], \quad (3)
$$

where the tilde symbol implies the Fourier transform and c_0 is a normalized dimensionless constant. One can easily tell that Eq. (3) is basically the Fourier spectrum of Airy beams with the coordinate transformation shown in Eq. (2). The real part and the imaginary part in Eq. (3) imply that the amplitude modulation and the phase modulation need to be involved in the corresponding experimental realization, respectively.

Of particular interest is the extension of quasi-Airy beams from the fully coherent case to its partially coherent counterpart. Figure 1 illustrates a schematic diagram for generation of PCQA beams. Let us consider a fluctuating, second-order field at the source plane. The cross-spectral density (CSD) function, if using Gaussian Schell-model sources, can be defined as a two-point correlation function [4]:

$$
\widetilde{W}_s(\mathbf{r_1'}, \mathbf{r_2'}) = \langle \widetilde{\phi}_s^*(\mathbf{r_1'})\widetilde{\phi}_s(\mathbf{r_2'}) \rangle
$$
$$
= \widetilde{\phi}_s^*(\mathbf{r_1'})\widetilde{\phi}_s(\mathbf{r_2'})\exp[-(\mathbf{r_1'} - \mathbf{r_2'})^2/2\delta_\mu^2], \quad (4)
$$

where the CSD function is the description of the field in the space-frequency domain, i.e., in the front focal plane of the Fourier lens in Fig. 1; $\widetilde{\phi}_s(\mathbf{r_j'})$ denotes the complex electric field [represented by Eq. (3)] with $\mathbf{r_j'} = (k_{x_j}, k_{y_j})$, $j = 1, 2$; the asterisk and the angular bracket denote a complex conjugate
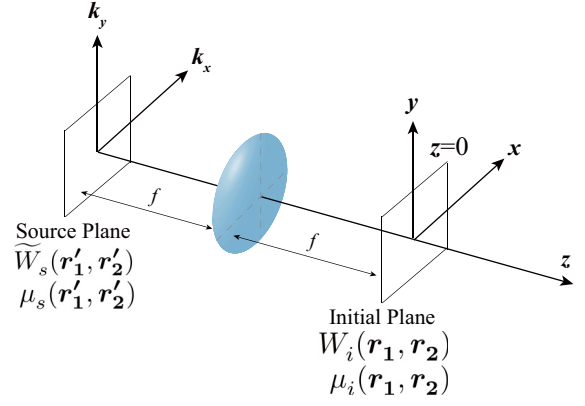

FIG. 1. Theoretical schematic for the radiation model of PCQA beams, which consists of the cross-spectral density function and DOC function at the source plane (labeled by s) and the initial plane (labeled by i) with a Fourier lens.

and an ensemble average, respectively; δ_μ is the source coherence length related to the spatial coherence width; the term $\exp[-(\mathbf{r_1'} - \mathbf{r_2'})^2/2\delta_\mu^2]$ is the Schell-model correlator. Equation (4) implies that we choose to impose the Schell-model correlation on the spectrum of quasi-Airy beams described by Eq. (3). Such a treatment is inspired by the pioneering work [18] in which the Airy beams are successfully extended from the coherent state to the incoherent one without any loss of acceleration range. Then, by employing Eq. (3) in Eq. (4), the complete expression for the CSD function of PCQA beams in the space-frequency domain can be written as

$$
\widetilde{W}_s(\mathbf{r_1'}, \mathbf{r_2'}) = \exp\left[-\frac{\alpha}{2}[\xi^2(\mathbf{r_1'}) + \eta^2(\mathbf{r_1'}) + \xi^2(\mathbf{r_2'}) + \eta^2(\mathbf{r_2'})]\right]
$$
$$
\times \exp\left[-\frac{ic_0^3}{3}[\xi^3(\mathbf{r_1'}) + \eta^3(\mathbf{r_1'}) - \xi^3(\mathbf{r_2'}) - \eta^3(\mathbf{r_2'})]\right]
$$
$$
\times \exp\left[-\frac{(\mathbf{r_1'} - \mathbf{r_2'})^2}{2\delta_\mu^2}\right]. \quad (5)
$$

Accordingly, the DOC function of PCQA beams can be examined by the following formula:

$$
\mu_s(\mathbf{r_1'}, \mathbf{r_2'}) = \frac{\widetilde{W}_s(\mathbf{r_1'}, \mathbf{r_2'})}{\sqrt{\widetilde{W}_s(\mathbf{r_1'}, \mathbf{r_1'})}\sqrt{\widetilde{W}_s(\mathbf{r_2'}, \mathbf{r_2'})}}
$$
$$
= \exp[-(\mathbf{r_1'} - \mathbf{r_2'})^2/2\delta_\mu^2]
$$
$$
\times \exp\left[-\frac{ic_0^3}{3}[\xi^3(\mathbf{r_1'}) + \eta^3(\mathbf{r_1'}) - \xi^3(\mathbf{r_2'}) - \eta^3(\mathbf{r_2'})]\right]. \quad (6)
$$

It is important to note that the imaginary part of Eq. (6) indicates the specific modulation of phase on the source. After being phase modulated, the source is no longer strictly Schell-model correlated because the DOC function cannot be written as the form of $\mu_s(\mathbf{r_1'} - \mathbf{r_2'})$. Still, the modulus of $\mu_s(\mathbf{r_1'}, \mathbf{r_2'})$ ranges between 0 and 1. Consequently, PCQA beams at $z = 0$ (i.e., at the initial plane) are derived from the
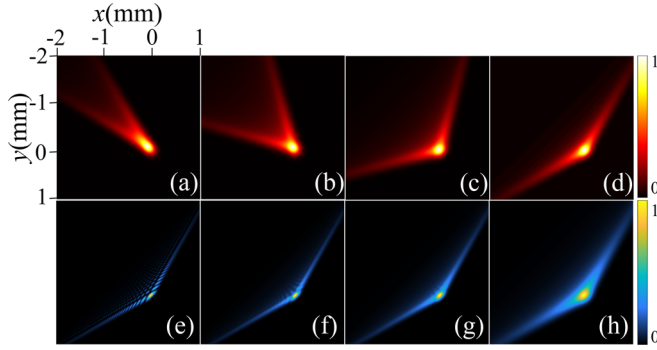
FIG. 2. Numerical simulation of the intensity distribution of PCQA beams at the initial plane ($z = 0$). (a–d) The intensity distribution with $\theta = 30°$, $60°$, $120°$, $150°$, respectively, for the source coherence lengths $\delta_\mu = 1$ mm. (e–h) The intensity distribution of PCQA beams with the source coherence lengths $\delta_\mu = \infty$, 3, 2 mm, 1 mm, respectively, for $\theta = 150°$. Other parameters are chosen as $\alpha = 0.025$, $w_0 = 1$ mm, and $\lambda = 532$ nm.

Fourier-transform formula [4,22]:

$$W_i(\mathbf{r_1}, \mathbf{r_2}) = \frac{k^2}{4\pi^2 f^2} \iint_{-\infty}^{\infty} \widetilde{W}_s(\mathbf{r'_1}, \mathbf{r'_2})$$
$$\exp\left[-\frac{ik(\mathbf{r_2} \cdot \mathbf{r'_2} - \mathbf{r_1} \cdot \mathbf{r'_1})}{f}\right] d^2\mathbf{r'_1}\, d^2\mathbf{r'_2}, \quad (7)$$

where $\mathbf{r_j} = (x_j, y_j)$, $j = 1, 2$ is an arbitrary position vector in the spatial domain; $k = 2\pi/\lambda$ is the wave vector with λ being the wavelength; f implies the focal length of a Fourier lens. It is worth mentioning that Eq. (5) implies the fields in the front focal plane of a Fourier lens while Eq. (7) denotes the fields in the rear focal plane as illustrated in Fig. 1. In other words, the fields of PCQA beams at the initial plane ($z = 0$) are constructed from the Fourier transform of Eq. (5).

Next, one can analyze the intensity distribution $S(\mathbf{r}, z = 0)$ of PCQA beams at $z = 0$, by applying Eq. (5) in Eq. (7) and setting $\mathbf{r_1} = \mathbf{r_2} = \mathbf{r}$. By choosing the source coherence length as $\delta_\mu = 1$ mm, we depict the intensity distribution of PCQA beams at the initial plane with the different initial angles θ in Figs. 2(a)–2(d). Here, we would like to emphasize that δ_μ refers to the coherence length of the source fields [described by Eq. (5)] at the source plane, rather than of PCQA beams [described by Eq. (7)] at the initial plane. From Figs. 2(a)–2(d), one can find that PCQA beams with both acute and obtuse initial angle perform a smooth profile and maintain a single lobe across two separate dimensions. In a special case when $\theta = 90°$, these PCQA beams turn into the previous case reported in [18]. Moreover, it is instructive to look at the conversion process of PCQA beams from the fully coherent state to the partially coherent one. In Figs. 2(e)–2(h), we exhibit the intensity distribution of PCQA beams at $z = 0$ with the source coherence length being $\delta_\mu = \infty$, 3 mm, 2 mm, and 1 mm, respectively. From Figs. 2(e)–2(h), one can see that when the source coherence length $\delta_\mu \to \infty$, the beam profile reduces to FCQA beams as shown in Fig. 2(e). Besides, the sidelobes of PCQA beams at the initial plane gradually disappear as δ_μ decreases. It is interesting to note that when $\delta_\mu = 1$ mm, the sidelobes vanish and the intensity converges on the mainlobe with the Airy tails as shown in Fig. 2(h).
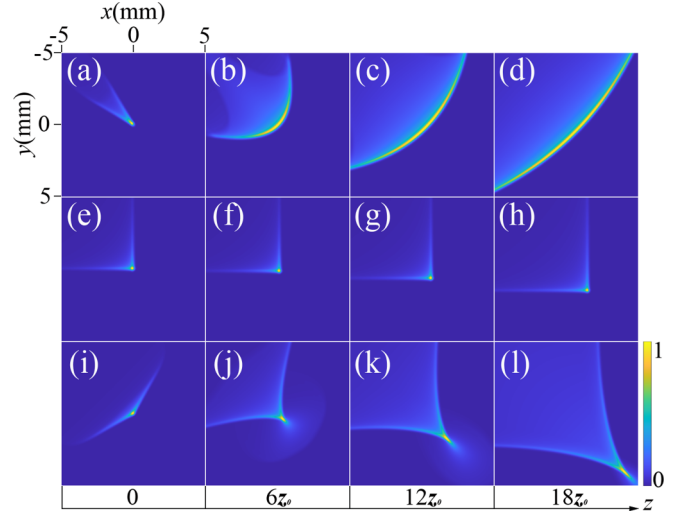

FIG. 3. The normalized transverse intensity distributions $S(\mathbf{r}, z)$ of PCQA beams at the different propagation distances for (a–d) $\theta = 30°$, (e–h) $\theta = 90°$, and (i–l) $\theta = 150°$. Other parameters are chosen as $w_r = 100$ μm, $\delta_\mu = 1$ mm, $\alpha = 0.025$, $w_0 = 1$ mm, and $\lambda = 532$ nm.

It is essential to examine the propagation dynamics of such a beam with the controllable initial angle between the two lobes. In the paraxial regime, the intensity distribution of PCQA beams in the half space $z > 0$ is acquired by the generalized Fresnel diffraction formula:

$$S(\mathbf{r}, z) = \iint_{-\infty}^{\infty} \widetilde{W}_s(\mathbf{r'_1}, \mathbf{r'_2}) P_z^*(\mathbf{r}, \mathbf{r'_1}, z) P_z(\mathbf{r}, \mathbf{r'_2}, z)\, d^2\mathbf{r'_1} d^2\mathbf{r'_2}, \quad (8)$$

where the propagation kernel P_z in an $ABCD$ optical system is

$$P_z(\mathbf{r}, \mathbf{r'}, z) = -ik/(2\pi B) \exp(ikz)$$
$$\times \exp\left(\frac{ikA}{2B}\mathbf{r'^2} - \frac{ik}{B}\mathbf{r'} \cdot \mathbf{r} + \frac{ikD}{2B}\mathbf{r^2}\right), \quad (9)$$

with the A, B, C, and D elements of the transfer matrix in our case being described as

$$\begin{pmatrix} A & B \\ C & D \end{pmatrix} = \begin{pmatrix} 1 & f+z \\ 0 & 1 \end{pmatrix} \begin{pmatrix} 1 & 0 \\ -1/f & 1 \end{pmatrix}$$
$$\times \begin{pmatrix} 1 & f \\ 0 & 1 \end{pmatrix} = \begin{pmatrix} -z/f & f \\ -1/f & 0 \end{pmatrix}. \quad (10)$$

Note that the $ABCD$ optical matrix implies the combination of the Fourier transform of Eq. (5) and the Fresnel diffraction of PCQA beams from the initial plane $z = 0$. Here, the propagation distance is measured in units of the Rayleigh range $z_0 = kw_r^2/2$ with the characteristic transverse width of the beams $w_r = c_0 f / kw_0$ [22]. By employing Eq. (5) in Eq. (8), the evolution of PCQA beams with the different θ during propagation from 0 to $18z_0$ is numerically simulated in Fig. 3. When $0 < \theta < 90°$, the two lobes of PCQA beams spread as a pair of wings during propagation. In the far field, the mainlobe expands to become a slim bar from an intensive spot. When $90° < \theta < 180°$, in contrast, the mainlobe constricts to be a narrow needlelike shape in the far field. To give an

explanation of these deformations in quantification, we recall the wavefront expression of a cubic-phase-modulated light beam presenting the Seidel coma wave aberration [33] and exercise it in our case:

$$\xi^3(k_x, k_y) + \eta^3(k_x, k_y) = \gamma_x \frac{k_x^3}{w_0^3} + \gamma_y \frac{k_y^3}{w_0^3} + \nu_x \frac{k_x^2 k_y}{w_0^3} + \nu_y \frac{k_x k_y^2}{w_0^3},$$
(11)

with

$$\gamma_x = \gamma_y = \sin^3 \frac{\varphi}{2} + \cos^3 \frac{\varphi}{2},$$
(12)

$$\nu_x = \nu_y = \frac{3}{2} \sin \varphi \left(\sin \frac{\varphi}{2} + \cos \frac{\varphi}{2} \right),$$
(13)

where γ_x and γ_y implement joint modulation with c_0 in Eq. (3) for the cubic phase; ν_x and ν_y represent the scales of comatic aberration along x and y axes in this light beam, respectively. Although the analysis is based on fully coherent light beams, it is valid for partially coherent fields even under the nearly incoherent state with random phase delays [34]. Therefore, the unusual propagation of PCQA beams shown in Fig. 3 results from the introduction of the optical caustic catastrophe induced by the Seidel coma. From this viewpoint, one can expect that when $\theta = 90°$ ($\varphi = 0$) these effects of aberration vanish due to the scales $\nu_x = \nu_y = 0$. In this case, as shown in Figs. 3(e)–3(h), the intensity distribution of PCQA beam remains shape preserving during propagation. The numerical solution for the CSD function of PCQA beams during propagation is derived in the Appendix.

III. COHERENT-MODE REPRESENTATION OF PCQA BEAMS

In this section, we focus on the coherent-mode representation of PCQA beams. A complex field $U(\mathbf{r})$ is determined by specific amplitude and phase function for a coherent light beam owing to the stationary fluctuation. For a stochastic light field, however, $U(\mathbf{r})$ becomes a random envelope, and thus it is more promising to represent the field with the ensemble average of $U(\mathbf{r})$. We first consider the light field in our case at $z = 0$, i.e., at the initial plane of Fig. 1, as the expression

$$W_i(\mathbf{r_1}, \mathbf{r_2}) = \langle U_i^*(\mathbf{r_1}) U_i(\mathbf{r_2}) \rangle,$$
(14)

where the asterisk and sharp bracket denote the complex conjugate and ensemble average, respectively. According to the multidimensional version of Mercer's theorem [4], such a CSD function can be decomposed into an incoherent sum of spatially coherent modes (or pseudomodes) $\psi_n(\mathbf{r})$ as

$$W_i(\mathbf{r_1}, \mathbf{r_2}) = \sum_n \chi_n \psi_n^*(\mathbf{r_1}) \psi_n(\mathbf{r_2}),$$
(15)

where χ_n is the weight function describing the contribution of each nth spatial mode $\psi_n(\mathbf{r})$ to $W_i(\mathbf{r_1}, \mathbf{r_2})$. The intensity distribution of PCQA beams at $z = 0$ is then written as

$$S(\mathbf{r}, z = 0) = \sum_n \chi_n |\psi_n(\mathbf{r})|^2.$$
(16)

From a mathematical viewpoint, χ_n are the eigenvalues and $\psi_n(\mathbf{r})$ are the eigenfunctions of the homogeneous Fredholm integral equation of the second kind [35], i.e.,

$$\int_{-\infty}^{\infty} W_i(\mathbf{r_1}, \mathbf{r_2}) \psi_n(\mathbf{r_1}) d^2 \mathbf{r_1} = \chi_n \psi_n(\mathbf{r_2}),$$
(17)

where $W_i(\mathbf{r_1}, \mathbf{r_2})$ has been treated as a kernel function with discretizing variables. However, deducing a coherent-mode structure from Eq. (17) with an exact solution is a highly sophisticated task. Even for the well-established Gaussian Schell-model light source, its coherent-mode representation is obtained in a closed form [35].

On the other hand, Gori and Palma proposed that, if we only focus on the intensity distribution, a Gaussian Schell-model beam can be considered as a superposition of an infinite number of coherent Gaussian modes [36]. These Gaussian modes are mutually incoherent on time average and separated by a random transverse shift in spatial coordinates. Along similar lines, Lumer *et al.* theoretically and experimentally proved that a partially coherent Airy beam can be constructed from an arbitrary number of coherent Airy modes [18], where all the modes have the same acceleration but are transversely shifted in spatial coordinates. Still, such a superposition law holds for the intensity distribution only. Enlightened by these studies, we introduce arbitrary transverse shifts Δ_{xn} and Δ_{yn}, respectively, in the x and y directions of fully coherent quasi-Airy modes [$\phi_i(x, y)$ in Eq. (1)], to form the coherent-mode structure of a partially coherent field at $z = 0$:

$$\begin{aligned} \psi_n(\mathbf{r}) &= \phi_i(x - \Delta_{xn}, y - \Delta_{yn}) \\ &= \text{Ai}[\xi(x - \Delta_{xn}, y - \Delta_{yn})] \text{Ai}[\eta(x - \Delta_{xn}, y - \Delta_{yn})], \end{aligned}$$
(18)

where the decay parameter and the chirp coefficient have been omitted for brevity. Assuming that both Δ_{xn} and Δ_{yn} are uniformly distributed random numbers in the interval $[-1, 1]$, the intensity distribution $|\psi_n(\mathbf{r})|^2$ for each nth mode can be obtained with each different value of $(\Delta_{xn}, \Delta_{yn})$. Figure 4(a) presents $|\psi_n(\mathbf{r})|^2$. For comprehensible presentation, we depict $|\psi_n(\mathbf{r})|^2$ with $(\Delta_{xn}, \Delta_{yn}) = (-1, -1), (1, -1), (0, 0), (-1, 1),$ and $(1, 1)$ as examples in Fig. 4(a). In that case, it is obvious that the weight function χ_n and the index n jointly determine the statistical properties of the field featured by the DOC function. For instance, when $\chi_n = 1$ for a single mode, the fields described by Eq. (15) are fully coherent since the corresponding DOC function is unimodular, i.e., $|\mu_i(\mathbf{r_1}, \mathbf{r_2})| = 1$. Therefore, to extract the complete expression of χ_n in Eqs. (15) and (16), one may first search for the DOC function of PCQA beams at $z = 0$, which can reflect the spatially statistical correlation between every shifted quasi-Airy mode. Since $W_i(\mathbf{r_1}, \mathbf{r_2})$ is a numerical solution with the double integrals (presented in the Appendix), the typical relation $\mu_i(\mathbf{r_1}, \mathbf{r_2}) = \frac{W_i(\mathbf{r_1}, \mathbf{r_2})}{\sqrt{S(r_1, z=0)}\sqrt{S(r_2, z=0)}}$ is impractical for derivation of $\mu_i(\mathbf{r_1}, \mathbf{r_2})$. We thus resort to the van Cittert–Zernike theorem [37] under the Fraunhofer approximation:

$$\mu_i(\mathbf{r_1}, \mathbf{r_2}) = \frac{k^2}{4\pi^2 f^2} \int_{-\infty}^{\infty} \widetilde{W}_s(\mathbf{r'}, \mathbf{r'}) \exp\left[-\frac{ik\mathbf{r'}(\mathbf{r_2} - \mathbf{r_1})}{f} \right] d^2\mathbf{r'},$$
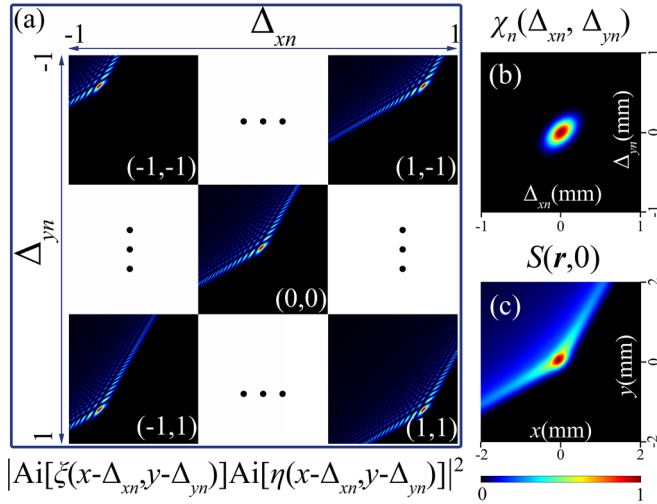(19)

FIG. 4. (a) The intensity distribution $|\psi_n(\boldsymbol{r})|^2$ of FCQA modes with different transverse shifts in the x and y directions at the initial plane. (b) The distribution of the weight function corresponding to different transverse shifts in spatial coordinates for each nth mode. (c) The intensity distribution $S(\boldsymbol{r}, z = 0)$ in Eq. (16). Other parameters are chosen as $w_0 = 1$ mm, $f = 750$ mm, and $\lambda = 532$ nm.

where $\widetilde{W}_s(\boldsymbol{r}', \boldsymbol{r}')$ is the source intensity distribution derived from Eq. (5). Equation (19) is a significant formula in coherence theory, revealing that the DOC function of the far field is proportional to the two-dimensional Fourier transform of the intensity distribution across the source. By employing Eq. (5) with $\boldsymbol{r}'_1 = \boldsymbol{r}'_2 = \boldsymbol{r}'$ into Eq. (19), we see at once that

$$\mu_i(x_d, y_d) = A_0 \exp\left(-\frac{x_d^2}{\sigma_x^2} - \frac{y_d^2}{\sigma_y^2} + \frac{x_d y_d}{2\sigma_{xy}^2}\right), \quad (20)$$

with

$$\sigma_x = \left(\frac{2f}{k w_0}\right)(1 + \tan^2\varphi)^{-\frac{1}{2}},$$

$$\sigma_y = \left(\frac{2f \cos\varphi}{k w_0}\right), \quad (21)$$

$$\sigma_{xy} = \left(\frac{f \cos\varphi}{k w_0}\right)(\sin\varphi)^{-\frac{1}{2}},$$

where A_0 is a normalized constant; the variables $(x_d, y_d) = (x_2 - x_1, y_2 - y_1)$ represent separations between two arbitrary points (x_1, y_1) and (x_2, y_2). One can find from Eq. (20) that when $\theta \neq 90°$ ($\varphi \neq 0$), the DOC function of PCQA beams at $z = 0$ performs the elliptical Gaussian distribution. To match such an elliptical Gaussian random process [38], we introduce a trial solution for the weight function χ_n by replacing (x_d, y_d) in $\mu_i(x_d, y_d)$ with $(\Delta_{xn}, \Delta_{yn})$:

$$\chi_n(\Delta_{xn}, \Delta_{yn}) = \mu_i(\Delta_{xn}, \Delta_{yn}). \quad (22)$$

Figure 4(b) illustrates the distribution of the weight function. Until now, as the required mode representation [Eq. (18)] and the weight function [Eq. (22)] are characterized, the coherent-mode representation of PCQA beams at $z = 0$ has been determined. By employing Eqs. (18) and (22) in Eq. (16), the intensity distribution of PCQA beams with $\theta = 150°$ at
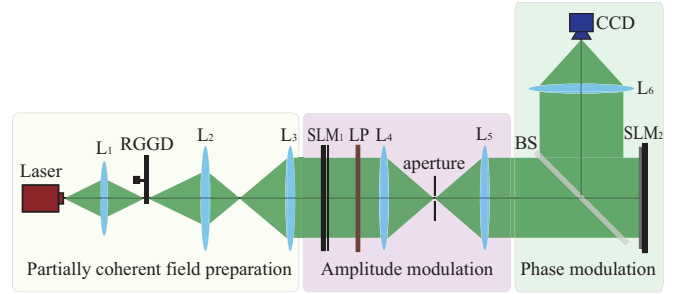
FIG. 5. Experimental schematic for generating the PCQA beams and detecting their intensity distribution. L_1, L_2, L_3, L_4, L_5, and L_6, lenses; RGGD, rotating ground-glass disk; LP, linear polarizer; SLM_1 and SLM_2, spatial light modulators; BS, beam splitter; CCD, charge-coupled device. The focal lengths of lenses are $f_1 = 100$ mm, $f_2 = f_3 = 150$ mm, $f_4 = f_5 = 300$ mm, and $f_6 = 750$ mm.

$z = 0$ is presented in Fig. 4(c). A straight comparison with Fig. 2(d) proves that there exists consistency between the two theoretical models, respectively, described by Eqs. (7) and (15). In addition, when $\theta = 90°$ ($\varphi = 0$), χ_n becomes a Gaussian distribution and $S(\boldsymbol{r}, z = 0)$ accordingly reduces to the previous results reported in [18]. It should be noted that the value range of Δ_{xn} and Δ_{yn} is not limited to the interval $[-1, 1]$. The simulation in Fig. 4(c) can still be reproduced by choosing other intervals for the transverse shifts Δ_{xn} and Δ_{yn} in spatial coordinates, as long as they are weighted by the distribution in Eq. (22).

From Eqs. (15)–(22), such a coherent-mode representation has a natural physical interpretation: the intensity distribution of a PCQA beam is constructed from a weighted sum of intensity distribution of a series of FCQA modes with random transverse displacements in spatial coordinates. The weight function implies the contribution of each mode. Thus, one may state the fact that some of the conclusions in the investigations about FCQA beams are still valid in a partially coherent field, including the dependence of the acceleration with the initial angle. In addition, the intensity distribution of PCQA beams during propagation can be obtained in a similar fashion by choosing the coherent modes $\psi_n(\boldsymbol{r}, z)$ at a certain propagation distance.

IV. EXPERIMENTAL REALIZATION

In this section, we carry out the experiment for generation and detection of PCQA beams. The experimental setup is established in Fig. 5. A linearly polarized Gaussian beam emitted from a semiconductor laser ($\lambda = 532$ nm) is first focused on a rotating ground-glass disk to effectively produce the partially coherent beams with the DOC function of Gaussian Schell-model form by a lens (L_1). By adjusting the position of the lens L_1 [4], we tailor the source coherence length to the case $\delta_\mu = 1$ mm. These beams are collimated into the SLM_1 (LC2012, Holoeye) and then go through a linear polarizer the polarization axis of which is perpendicular to the polarization direction of incident light for the functioning of this SLM_1. In our implementation, SLM_1 plays the role of a filter to modulate the amplitude of light. Subsequently, the amplitude-modulated beams pass through a $4f$ optical
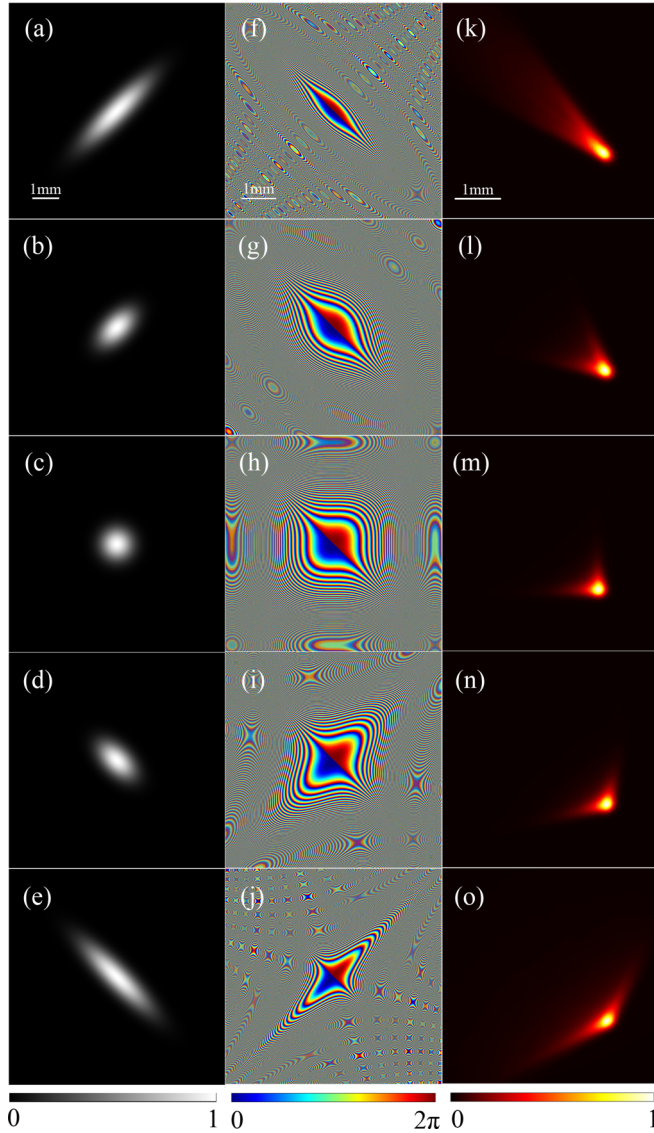
FIG. 6. Experimental results for generation of PCQA beams and the corresponding detection. (a–e) The amplitude patterns imposed on SLM_1. (f–j) The phase patterns imposed on SLM_2. (k–o) The generation of PCQA beams at $z = 0$ with $\theta = 30°, 60°, 90°, 120°, 150°$ between the two lobes, respectively.
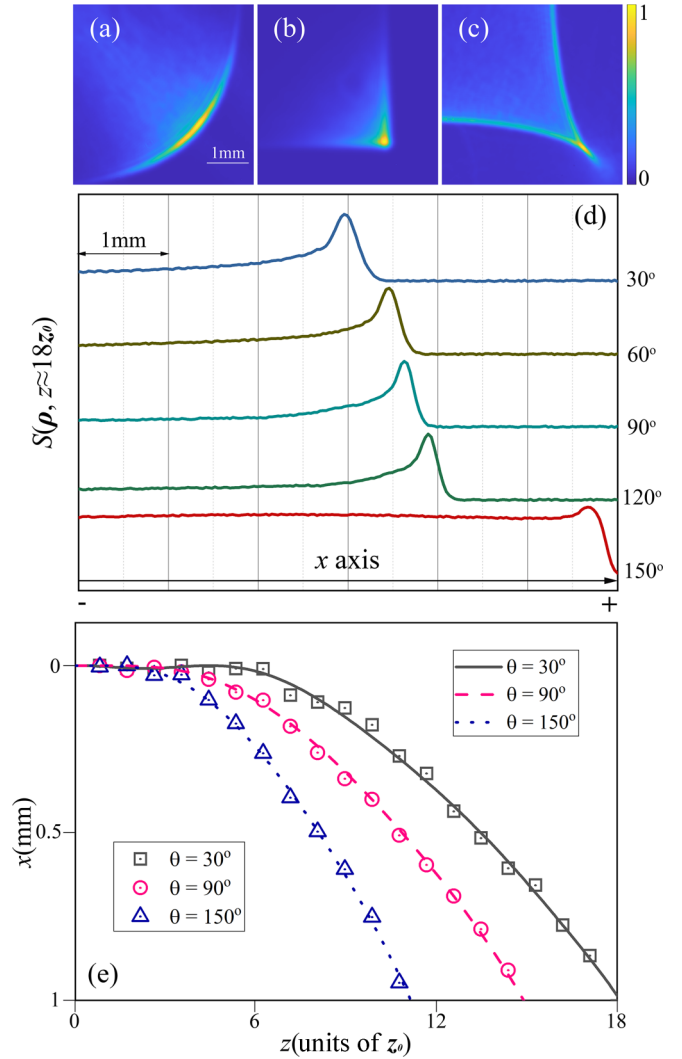

FIG. 7. The experimental detection of the intensity distribution of PCQA beams at the plane $z \approx 18z_0$ for the cases of (a) $\theta = 30°$, (b) $\theta = 90°$, and (c) $\theta = 150°$; (d) their one-dimensional distribution projecting on the x axis at $z \approx 18z_0$; (e) acceleration range marked by peak intensity in the mainlobe of PCQA beams for different θ during propagation from 0 to $18z_0$. The curves and patterns denote theoretical predictions and experimental results, respectively.

system consisting of a pair of lenses (L_4 and L_5) with an aperture, in order to remove the lattice diffraction from liquid crystal. Afterwards the phase information is imposed on the beams by the SLM_2. The phase-modulated beams go through a two-dimensional Fourier transform with a Fourier lens (L_6) and finally reach a CCD for detection.

According to Eq. (3), the modulation of amplitude and phase should be synchronized with each other in the generation of PCQA beams. The imposed patterns on SLM_1 [Figs. 6(a)–6(e)] and SLM_2 [Figs. 6(f)–6(j)] are depicted by calculating real and imaginary parts of Eq. (3), respectively. Each row of Fig. 6 represents the generation and the detection in a single experiment. For instance, matching the amplitude patterns in Fig. 6(e) with the phase patterns in Fig. 6(j) makes the realization of the PCQA beam at $z = 0$ with $\theta = 150°$

shown in Fig. 6(o). It is interesting to conclude that with the increasing of θ, the amplitude patterns seem to become elliptical Gaussian or Gaussian distributions while the phase patterns are stretched along the diagonal. What is more, the experimental results in Fig. 6 are in an agreement with the numerical simulation in Fig. 2.

The experimental demonstration of beam shaping for PCQA beams with various θ is presented in Figs. 7(a)–7(c). To investigate their acceleration properties, we examine the one-dimensional distribution of the intensity distribution projecting on the x axis at $z \approx 18z_0$ in Fig. 7(d), by fixing the location of CCD and successively changing the corresponding patterns on SLM_1 and SLM_2. Note that the plot shown in Fig. 7(d) can be considered as the side view of PCQA beams at a specific plane. From Fig. 7(d) one can see that PCQA beams with the different initial angle retain the

properties of smooth profile and sole local maximum during propagation. Moreover, PCQA beams with $\theta = 150°$ experience an earlier deformation compared to those with $\theta = 30°$. This phenomenon indicates that the comatic aberration has a greater impact on the propagation of the beams with obtuse initial angle. Furthermore, in Fig. 7(d), it is clear to find that as the initial angle increases, the direction of the mainlobe moves along the positive x axis. From these phenomena we deduce that varying the initial angle θ can lead to the different accelerating curves of PCQA beams. For the verification of this deduction, we numerically simulate peak intensity of the mainlobe of the beams during propagation, and experimentally collect the corresponding data. Figure 7(e) shows that the propagation trajectory of PCQA beams performs a parabolic-type curve as the well-known Airy beams. Moreover, by comparing the slopes of these curves, we find that the acceleration of PCQA beams reduces with the decreasing of θ. More information about the dependence of acceleration properties of PCQA beams with different θ can be found in the Appendix. Therefore, on the basis of the above analyses, we can draw a conclusion that adjusting the initial angle of PCQA beams allows the control of the propagation properties effectively, such as the acceleration and the beam shape.

V. CONCLUSIONS

In summary, we theoretically and experimentally report on an alternative class of partially coherent light beams with controllable acceleration. They are originated by imposing specific amplitude and phase information on a Gaussian Schell-model source in the spatial frequency domain. Those beams, at the plane $z = 0$, exhibit a prearranged initial angle between their two lobes. As the source coherence length decreases, the sidelobes of the beams gradually disappear and the intensity smoothly concentrates on the mainlobe with the Airy tails. During propagation, the two lobes perform the action of expansion and constriction when the initial angle is acute and obtuse, respectively. It was pointed out that they can be engineered to propagate along various accelerating curves as long as the initial angle is properly chosen. In addition, owing to the comatic aberration, the transverse intensity pattern undergoes the deformation. Based on the coherent-mode representation, the intensity distribution of a PCQA beam can be considered as a weighted sum of intensity distribution of a number of FCQA beams with random transverse shifts in spatial coordinates. With the proposed experimental setup, our experimental results provide an agreement with the theoretical predictions.

We believe our paper may inspire new ideas in research associated with partially coherent light beams, and also widen the range of potential applications such as diffraction tomography [39] and speckle mitigation [40], where the spatial coherence properties of light can play an important role.

APPENDIX: NUMERICAL SOLUTION FOR THE RADIATION MODEL

In this section, we provide the complete expression for the radiation model of PCQA beams, and accordingly make the plots for PCQA beams with various θ, complementary to Fig. 7(e) in the main text. The CSD function of PCQA beams during propagation can be written as

$$W(\boldsymbol{r_1}, \boldsymbol{r_2}, z)$$
$$= \iint_{-\infty}^{\infty} \widetilde{W}_s(\boldsymbol{r'_1}, \boldsymbol{r'_2}) P_z^*(\boldsymbol{r_1}, \boldsymbol{r'_1}, z) P_z(\boldsymbol{r_2}, \boldsymbol{r'_2}, z) \, d^2\boldsymbol{r'_1} d^2\boldsymbol{r'_2}. \tag{A1}$$

On substituting from Eqs. (5) and (9) in Eq. (A1), and by integrating k_{x_1} and k_{y_2} of $\widetilde{W}_s(k_{x_1}, k_{y_1}, k_{x_2}, k_{y_2})$ with the formula [41],

$$\int_{-\infty}^{\infty} \exp\left[i\left(\frac{t^3}{3} + at^2 + bt\right)\right] dt$$
$$= 2\pi \, \mathrm{Ai}(b - a^2) \exp\left[i\left(\frac{2a^3}{3} - ab\right)\right], \tag{A2}$$

one can write down the numerical solutions as double integrals:

$$W(x_1, y_1, x_2, y_2, z)$$
$$= W_0 \iint_{-\infty}^{\infty} \mathrm{Ai}\left(\Lambda_{11}k_{x_2} + \Lambda_{21}k_{x_2}^2 + \Lambda_{31} - \frac{k(y_1 + y_2)}{2c_0 fm}\right)$$
$$\times \mathrm{Ai}\left(\Lambda_{12}k_{y_1} + \Lambda_{22}k_{y_1}^2 + \Lambda_{32} + -\frac{k(x_1 + x_2)}{2c_0 fm}\right)$$
$$\times \exp\left(\Xi_{11}k_{x_2} + \Xi_{21}k_{x_2}^2 + \Xi_{31}k_{x_2}^3\right)$$
$$\times \exp\left(\Xi_{12}k_{y_1} + \Xi_{22}k_{y_1}^2 + \Xi_{32}k_{y_1}^3\right)$$
$$\times \exp\left(-\frac{kz}{2f^2\delta_\mu^2 c_0^3 m^3}(k_{x_2} - k_{y_1})\right) dk_{x_2} dk_{y_1} \tag{A3}$$

where

$$\Lambda_{1j} = (-1)^j \frac{2\Psi\Upsilon_j(z)}{3c_0 m^4} - \frac{i\alpha\sin\varphi}{c_0 m w_0^2},$$

$$\Lambda_{2j} = (-1)^j \frac{\Psi c_0^2}{3m} - \frac{\Psi^2 c_0^2}{9m^2},$$

$$\Lambda_{3j} = \frac{ik_{y_1}^2}{c_0 m \delta_\mu^2} - \frac{\Upsilon_j^2(z)}{c_0^4 m^4} - \frac{k(y_1 + y_1)}{2c_0 fm},$$

$$\Xi_{1j} = i^{2j-1} \frac{2\Psi\Upsilon_j^2(z)}{3c_0^3 m^6} + \frac{\Omega w_0^2 + \alpha\delta_\mu^2 \sin\varphi\Psi\Upsilon_j(z)}{\delta_\mu^2 w_0^2 c_0^3 m^3},$$

$$\Xi_{2j} = \frac{i\Psi(3m^3 + 2\Psi)\Upsilon_j(z)}{9m^6} + (-1)^j \frac{\alpha\Psi\sin\varphi}{3w_0^2 m^3},$$

$$\Xi_{3j} = \frac{i\Psi^2 c_0^3}{9m^3} + i^{2j-1}\frac{2\Psi^3 c_0^3}{81m^6}, \tag{A4}$$
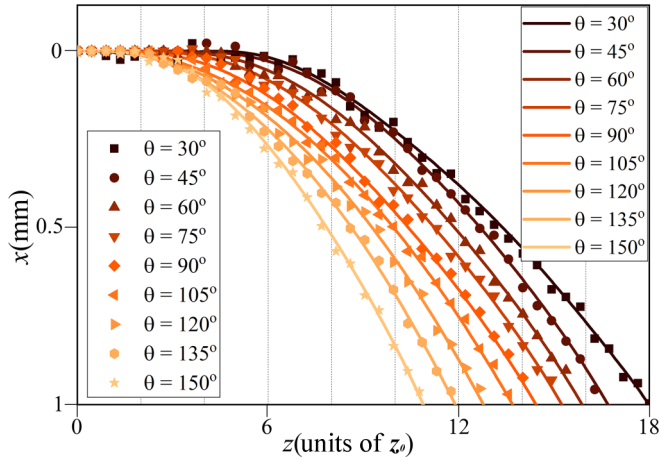
FIG. 8. Complementary plot for Fig. 7(e).

with

$$\Psi = \frac{3}{2} \sin \varphi \left(\sin \frac{\varphi}{2} + \cos \frac{\varphi}{2} \right),$$

$$\Omega = \frac{i\alpha}{2w_0^2} + \frac{i}{2\delta_\mu^2},$$

$$\Upsilon_j(z) = \Omega - i^{2j} \frac{kz}{2f^2},$$

$$j = 1, 2,$$

(A5)

where W_0 is a normalized constant; Ψ is a coefficient related to the comatic aberration as identical to ν_x and ν_y in Eq. (13). It is not difficult to tell that, setting $z = 0$ and $(x_1 = x_2, y_1 = y_2) = (x, y)$ in Eq. (A3), respectively, leads to Eqs. (7) and (8). Based on Eqs. (A3)–(A5), the acceleration range (marked by peak intensity) of PCQA beams with more values of θ is illustrated in Fig. 8, by utilizing numerical simulation and experimental results.

[1] B. M. Oliver, Sparkling spots and random diffraction, Proc. IEEE **51**, 220 (1963).

[2] J. W. Goodman, *Speckle Phenomena in Optics: Theory and Applications* (Roberts & Company, Greenwood Village, CO, 2007).

[3] B. Redding, M. A. Choma, and H. Cao, Speckle-free laser imaging using random laser illumination, Nat. Photonics **6**, 355 (2012).

[4] L. Mandel and E. Wolf, *Optical Coherence and Quantum Optics* (Cambridge University, Cambridge, England, 1995).

[5] E. Collett and E. Wolf, Is complete coherence necessary for generation of highly directional light-beams? Opt. Lett. **2**, 27 (1978).

[6] O. Korotkova and G. Gbur, Applications of optical coherence theory, Prog. Opt. **65**, 43 (2020).

[7] D. M. Palacios, I. D. Maleev, A. S. Marathay, and G. A. Swartzlander, Spatial Correlation Singularity of a Vortex Field, Phys. Rev. Lett. **92**, 143905 (2004).

[8] W. Wang and M. Takeda, Coherence Current, Coherence Vortex, and the Conservation Law of Coherence, Phys. Rev. Lett. **96**, 223904 (2006).

[9] W. Wang, Z. Duan, S. G. Hanson, Y. Miyamoto, and M. Takeda, Experimental Study of Coherence Vortices: Local Properties of Phase Singularities in a Spatial Coherence Function, Phys. Rev. Lett. **96**, 073902 (2006).

[10] G. J. Gbur, *Singular Optics* (CRC, Boca Raton, FL, 2017).

[11] Y. T. Zhang, Y. J. Cai, and G. Gbur, Partially coherent vortex beams of arbitrary radial order and a van Cittert-Zernike theorem for vortices, Phys. Rev. A **101**, 043812 (2020).

[12] G. Gbur and T. D. Visser, Coherence vortices in partially coherent beams, Opt. Commun **222**, 117 (2003).

[13] L. Y. Ma and S. A. Ponomarenko, Optical coherence gratings and lattices, Opt. Lett. **39**, 6656 (2014).

[14] Y. H. Chen, S. A. Ponomarenko, and Y. J. Cai, Experimental generation of optical coherence lattices, Appl. Phys. Lett. **109**, 061107 (2016).

[15] E. Wolf and D. F. James, Correlation-induced spectral changes, Rep. Prog. Phys. **59**, 771 (1996).

[16] G. A. Siviloglou and D. N. Christodoulides, Accelerating finite energy Airy beams, Opt. Lett. **32**, 979 (2007).

[17] G. A. Siviloglou, J. Broky, A. Dogariu, and D. N. Christodoulides, Observation of Accelerating Airy beams, Phys. Rev. Lett. **99**, 213901 (2007).

[18] Y. Lumer, Y. Liang, R. Schley, I. Kaminer, E. Greenfield, D. Song, X. Zhang, J. Xu, Z. Chen, and M. Segev, Incoherent self-accelerating beams, Optica **2**, 886 (2015).

[19] J. E. Morris, M. Mazilu, J. Baumgartl, T. Cizmar, and K. Dholakia, Propagation characteristics of Airy beams: Dependence upon spatial coherence and wavelength, Opt. Express **17**, 13236 (2009).

[20] X. Chu, Evolution of an Airy beam in turbulence, Opt. Lett. **36**, 2701 (2011).

[21] H. T. Eyyuboğlu and E. Sermutlu, Partially coherent Airy beam and its propagation in turbulent media, Appl. Phys. B **110**, 451 (2012).

[22] Z. H. Pang and D. M. Zhao, Partially coherent dual and quad airy beams, Opt. Lett. **44**, 4889 (2019).

[23] N. K. Efremidis and D. N. Christodoulides, Abruptly autofocusing waves, Opt. Lett. **35**, 4045 (2010).

[24] D. G. Papazoglou, N. K. Efremidis, D. N. Christodoulides, and S. Tzortzakis, Observation of abruptly autofocusing waves, Opt. Lett. **36**, 1842 (2011).

[25] H. Zhong, Y. Zhang, M. R. Belić, C. Li, F. Wen, Z. Zhang, and Y. Zhang, Controllable circular Airy beams via dynamic linear potential, Opt. Express **24**, 7495 (2016).

[26] Y. Lumer, L. Drori, Y. Hazan, and M. Segev, Accelerating Self-Imaging: The Airy-Talbot Effect, Phys. Rev. Lett. **115**, 013901 (2015).

[27] Y. Zhang, H. Zhong, M. Belić, X. Liu, W. Zhong, Y. Zhang, and M. Xiao, Dual accelerating Airy-Talbot recurrence effect, Opt. Lett. **40**, 5742 (2015).

[28] Y. X. Qian and S. T. Zhang, Quasi-Airy beams along tunable propagation trajectories and directions, Opt. Express **24**, 9489 (2016).

[29] Y. Liang, Y. Hu, Z. Ye, D. Song, C. Lou, X. Zhang, J. Xu, R. Morandotti, and Z. Chen, Dynamical deformed Airy beams

with arbitrary angles between two wings, J. Opt. Soc. Am. A **31**, 1468 (2014).

[30] O. Vallée and M. Soares, *Airy Functions and Applications to Physics* (Imperial College, London, 2010).

[31] Y. Zhang, X. Liu, M. R. Belić, W. Zhong, Y. Zhang, and M. Xiao, Propagation Dynamics of a Light Beam in a Fractional Schrödinger Equation, Phys. Rev. Lett. **115**, 180403 (2015).

[32] Y. Zhang, M. R. Belić, J. Sun, H. Zheng, Z. Wu, and H. Chen, Controllable acceleration and deceleration of Airy beams via initial velocity, Rom. Rep. Phys **67**, 1099 (2015).

[33] H. H. Hopkins, *Wave Theory of Aberrations* (Oxford, New York, 1950).

[34] M. Born and E. Wolf, *Principles of Optics* (Cambridge University, Cambridge, England, 1999).

[35] A. Starikov and E. Wolf, Coherent-mode representation of Gaussian Schell-model sources and of their radiation fields, J. Opt. Soc. Am. **72**, 923 (1982).

[36] F. Gori and C. Palma, Partially coherent sources which give rise to highly directional laser beams, Opt. Commun. **27**, 185 (1978).

[37] F. Zernike, The concept of degree of coherence and its application to optical problems, Physica **5**, 785 (1938).

[38] D. Voelz, X. Xiao, and O. Korotkova, Numerical modeling of Schell-model beams with arbitrary far-field patterns, Opt. Lett. **40**, 352 (2015).

[39] P. S. Carney and E. Wolf, Power-excitation diffraction tomography with partially coherent light, Opt. Lett. **26**, 1770 (2001).

[40] E. N. Leith and J. Upatnieks, Wavefront reconstruction with diffused illumination and three-dimensional objects, J. Opt. Soc. Am. **54**, 1295 (1964).

[41] O. Vallée and M. Soares, *Airy Functions and Applications to Physics*, 2nd ed. (Imperial College, London, 2010).